Structural Characteristics of Natural-Gas-Vehicle-Aged Oxidation Catalyst

Mari Honkanen[1,*], Marja Kärkkäinen[2], Ville Viitanen[3], Hua Jiang[3], Kauko Kallinen[4], Mika Huuhtanen[2], Minnamari Vippola[1], Jouko Lahtinen[3], Riitta Keiski[2] and Toivo Lepistö[1]

[1] Department of Materials Science, Tampere University of Technology, P.O.Box 589, 33101 Tampere, Finland
[2] Mass and Heat Transfer Process Laboratory, University of Oulu, P.O.Box 4300, 90014 University of Oulu, Finland
[3] Department of Applied Physics, Aalto University, P.O.Box 11100, 00076 Aalto, Finland
[4] Ecocat Oy, Typpitie 1, 90620 Oulu, Finland

[*] Corresponding author, e-mail: mari.honkanen@tut.fi, telephone: +358408490133, fax number: +35833641426

Keywords: Pt/Pd catalyst, natural gas, deactivation, TEM, XRD, XPS

Abstract (180 words, based on the instructions for authors in the web page of Topics in Catalysis)

Deactivation of the natural-gas-vehicle-aged Pt/Pd oxidation catalyst supported on γ-alumina-based washcoat was studied by electron microscopy, X-ray diffractometry, X-ray photoelectron spectroscopy, and catalytic activity measurements. Significant structural changes were detected in the used catalyst compared to the fresh one. Grain size of the washcoat had grown but its structure had remained the same, γ-alumina, as in the fresh catalyst. Sintering of the noble metal particles had occurred, particle sizes varied from ~5 nm up to ~100 nm. Decomposition of palladium oxide and platinum oxide to metallic Pd and Pt occurred followed by the formation of the bimetallic Pt/Pd crystals. Also reformation of palladium oxide was detected. In addition, the inlet part of the used catalyst was totally covered by a poisoning layer. Due to these structural changes and poisoning, the activity of the vehicle-aged catalyst had decreased significantly compared to the fresh one. All the changes were stronger in the inlet than in the outlet part of the used catalyst indicating higher operating temperature and more extensive thermal deactivation and poisoning in the inlet than in the outlet part of the converter.

Abstract (78 words, based on the instructions for authors in the web page of the conference)

Deactivation of the natural-gas-vehicle-aged Pt/Pd oxidation catalyst supported on γ-alumina-based washcoat was studied. Sintering of the noble metal particles occurred during vehicle aging. Decomposition of palladium and platinum oxides to metallic Pd and Pt occurred followed by the formation of the bimetallic Pt/Pd crystals. Also reformation of palladium oxide was detected. The inlet part of the used catalyst was covered by a poison layer. The activity of the vehicle-aged catalyst had decreased significantly compared to the fresh one.

1. INTRODUCTION

Natural gas is a potential energy source to reduce pollution; lean-burn natural-gas engines have higher thermal efficiencies and cleaner exhaust gases than stoichiometric engines. The exhaust emissions of the natural gas vehicles (NGVs) still contain e.g. CO, NO_x, and unburned methane. NO_x emissions and particulates in the NGV exhaust gases are much lower than in the diesel vehicles but the disadvantage of the NGVs is unburned methane, a potent greenhouse gas, and thus catalytic converters are needed [1,2]. In addition of the stability of the methane molecule, the reaction conditions of the NGV engine exhausts are challenging for the catalytic after-treatment. Generally engine exhausts of the lean NGVs have: low temperature (<500–550°C), low CH_4 concentrations (500–1000 ppm), large amounts of water vapour (10–15 %) and CO_2, high excess of oxygen, and presence of SO_x and NO_x [1]. Supported palladium catalysts are widely known to be active for methane combustion in the mentioned reaction conditions. Most researchers, like [3–5], agree that PdO is the active phase of a palladium catalyst for methane oxidation while metallic palladium is much less active. Support materials used in methane combustion catalysts are usually alumina, titania, silica, zirconia, and their mixtures [6,7].

Deactivation of the catalyst, caused by e.g. poisoning, fouling, and thermal degradation and sintering, is a problem also in the natural gas engine applications. For example sulfur-containing compounds cause poisoning of Pd-catalysts resulting in inhibition of the methane combustion activity and deactivation of the catalyst [8–10]. In general, the activity of Pd-catalysts decreases when the active phase, i.e. PdO decomposes to metallic Pd [3–5] and also when PdO sinters [11,12]. Pd « PdO transformation is reversible and according to Farrauto *et al.* [4], decomposition temperature of PdO to Pd in the PdO/Al_2O_3 catalyst was ~800°C and reformation temperature of Pd to PdO during cooling was ~600°C. Hysteresis in the reformation is due to strongly bound oxygen on the Pd surface inhibiting bulk oxidation [5]. However, many factors, such as gas phase

composition and pressure, type of support, additives and contaminants, and pretreatment history, have effects on Pd « PdO transformation [6].

Several studies have reported that the activity and stability of Pd-catalysts in methane combustion can be improved by adding Pt into the catalyst [12–18]. This is due to the fact that Pt decelerates sintering of Pd and PdO [12,15,18]. However, Castellazzi *et al.* [19] have reported that the effect of Pt on the Pt-Pd/Al_2O_3 catalyst in methane combustion is not straightforward; Pt can act as an inhibitor or promoter of catalytic activity depending on several factors such as: extent of PdO formation, strength of Pd and the support interactions, and stabilization of metallic Pd. This means that it is important to study deactivation phenomena of the potential Pt/Pd catalysts for natural gas applications. Challenges in the catalysts used in natural gas applications are even more demanding than e.g. in diesel applications due to the sensitivity of methane performance for thermal and especially for chemical aging.

The aim of this study was to characterize structural changes in a commercial natural-gas-vehicle-aged Pt/Pd oxidation catalyst supported on g-alumina-based washcoat compared to the fresh one. Deactivation mechanism in the used catalyst was studied by electron microscopy, X-ray diffractometry, X-ray photoelectron spectroscopy, and with catalytic activity and specific surface area measurements.

2. EXPERIMENTAL

2.1. Studied catalyst

The Pt/Pd (1:4) catalyst supported on the γ-alumina-based washcoat manufactured and designed by Ecocat Oy for natural gas applications was characterized. The catalyst was studied as fresh and after lean-burn natural-gas-heavy-duty-vehicle aging (160 000 km). The inlet, middle, and outlet parts of the aged catalyst were studied.

2.2. Microstructural characterization

The fresh and vehicle-aged catalysts were studied by field emission gun scanning electron microscopy (FEGSEM), transmission electron microscopy (TEM), X-ray diffractometry (XRD), and X-ray photoelectron spectroscopy (XPS). FEGSEM (Zeiss ULTRAplus) is equipped with energy dispersive spectrometer (EDS, INCA Energy 350 with INCAx-act silicon-drift (SDD)) detector, Oxford Instruments). Cross-sectional FEGSEM samples were prepared with conventional metallographic sample preparation technique. All the presented FEGSEM images were taken with an angular selective backscatter (AsB) detector. TEM (Jeol JEM-2010) is equipped with EDS (Noran Vantage Si(Li) detector, Thermo Scientific). Field emission gun high resolution (scanning) transmission electron microscope (FEG HR(S)TEM, JEOL-2200FS) is integrated with two aberration correctors (CEOS GmbH) for both the TEM image-forming and the STEM probe-forming lenses. It is also equipped with EDS (Si(Li) detector, Jeol) and an in-column Omega-type energy filter (Jeol) facilitating the electron energy loss spectrometry (EELS) and energy-filtered TEM (EFTEM). Samples for TEM studies were prepared by crushing the scraped catalyst powder between two laboratory glass slides and dispersing the crushed powder with ethanol onto a copper grid with a holey carbon film. For FEGSEM and TEM studies, the vehicle-aged catalyst was divided to nine samples from inlet to outlet to study the structural changes in various part of the used catalyst (Fig. 1). Scraped catalyst powder was also used for XRD (D5000, Siemens, using Cu Kα radiation) studies and

measurements were carried out for the fresh catalyst and for the inlet, middle, and outlet part of the vehicle-aged catalyst (Fig. 1). The phases were identified by using the JCPD database (International Center for Diffraction Data (ICDD), Powder Diffraction File Database 1999). For XPS (SSX-100, Surface Science Instruments, using monochromatic Al Ka radiation) studies, a small amount of the scraped catalyst powder was pressed into a piece of indium and the samples were pretreated in high vacuum for a few hours before measurements. XPS measurements were carried out for the fresh and for the inlet and outlet parts of the vehicle-aged catalyst (Fig 1). The binding energy reference for XPS measurements was the O 1s peak at 531.0 eV.

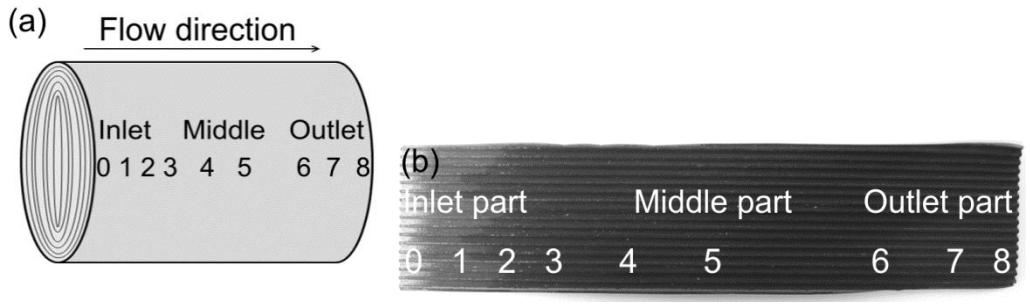

Fig. 1 Studied positions of the vehicle-aged catalyst (total length 150 mm) marked to the (a) schematic drawing and (b) image of the studied catalyst foil, FEGSEM and TEM studies were carried out for nine positions from the inlet (0) to the outlet (8); XRD spectra were recorded for the inlet (positions 0–3), middle (positions 4–5), and outlet parts (positions 6–8); XPS studies were carried out for the inlet (positions 0–3) and outlet parts (positions 6–8), specific surface area, average pore size and volumes were determined for the inlet (positions 0–3), middle (positions 4–5), and outlet parts (positions 6–8), and catalytic activities were measured for the inlet (positions 0–3) and outlet parts (positions 6–8)

2.3. Catalytic activity and catalyst surface area measurements

Catalytic activities of the fresh and the inlet and outlet parts of the vehicle-aged (Fig. 1) monolith catalyst were measured with laboratory-scale light-off experiments with the following gas mixture: 600 ppm CH_4, 500 ppm CO, 10 vol-% CO_2, 12 vol-% O_2, and 10 vol-% H_2O, and N_2 as balance gas. The sample was placed in a quartz-tube and the measurements were carried out in a tubular furnace at atmospheric pressure. The total gas flow was 1 dm^3/min resulting in a gas hourly space velocity (GHSV) of 31000 h^{-1} for a monolith sample having the diameter and length of 0.8 cm and 3.8 cm, respectively. The gas flow was controlled by mass flow controllers (Brooks 5850TR). H_2O was added into the reactor at 110°C with a peristaltic pump. Temperature of the catalyst sample was increased from room temperature (RT) to 600°C with a heating rate 10°C/min. Concentrations of the feed and product gases were measured as a function of temperature every five seconds by Gasmet™ FT-IR gas analyzer. Oxygen concentration was determined by using a paramagnetic oxygen analyzer (ABB Advanced Optima).

Specific surface area and average pore size and volume of the fresh catalyst and samples taken from the inlet, middle, and outlet parts of the aged catalyst (Fig. 1) were determined by nitrogen adsorption at -196°C with the Micrometrics ASAP 2020 analyzer. Specific surface area was calculated according to the Brunauer-Emmett-Teller (BET) theory and the average pore sizes and volumes were determined using the Barrett-Joyner-Halenda (BJH) theory of nitrogen isotherm analysis.

3. RESULTS AND DISCUSSION

3.1. Microstructural characterization

Cross-sections of the catalysts were studied with FEGSEM and images with two magnifications of the fresh catalyst and the inlet part and the middle part of the used catalyst are presented in Fig. 2. In the fresh catalyst, Pt/Pd particles were too small to be detected by FEGSEM (Fig. 2 (a)). Particle size of Pt/Pd increased through the catalyst in the vehicle-aging (white spots in Figs. 2 (b) and (c)), but noble metals were still well distributed in the cross-sections of the used catalyst. The middle part and the outlet part (not shown) looked similar. Particle size decreased from the inlet part to the outlet part. According to the EDS studies, the inlet part of the used catalyst (position 0, Fig. 1) was totally covered by a Ca-, P-, and S-rich layer (marked as poison layer in Fig. 2 (b)) and phosphorus had also penetrated in the top layer of the catalyst (brighter layer on the top of the catalyst, marked as P penetrated in Fig. 2 (b)). The poison layer was detected only in the very inlet part of the catalyst (sample 0, Fig. 1). More detailed elemental analysis of the fresh and used catalysts was carried out with XPS. Poisoning elements were detected in the used catalyst: the amount of these elements (in weight-%) in the inlet part (poison layer + washcoat) were c/Ca » 19, c/S » 12, c/P » 8, c/Zn » 5, and c/Si » 0.8 and in the outlet part c/Ca » 0.8, c/S » 1.3, c/P » 0.2, c/Zn » 0.1, and c/Si » 0.1. FEGSEM and XPS studies indicated clearly that the poisoning decreased significantly from the inlet part to the outlet part.

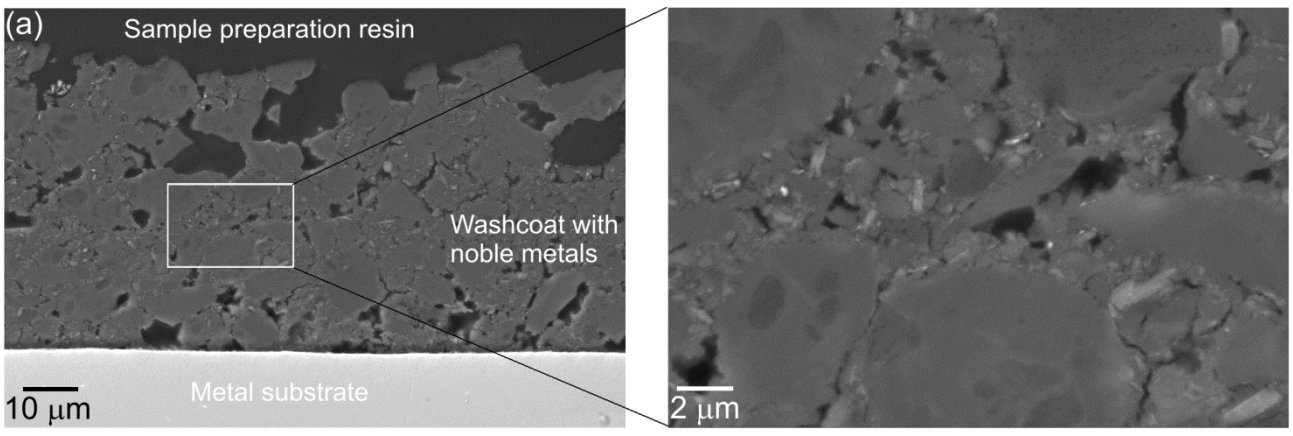

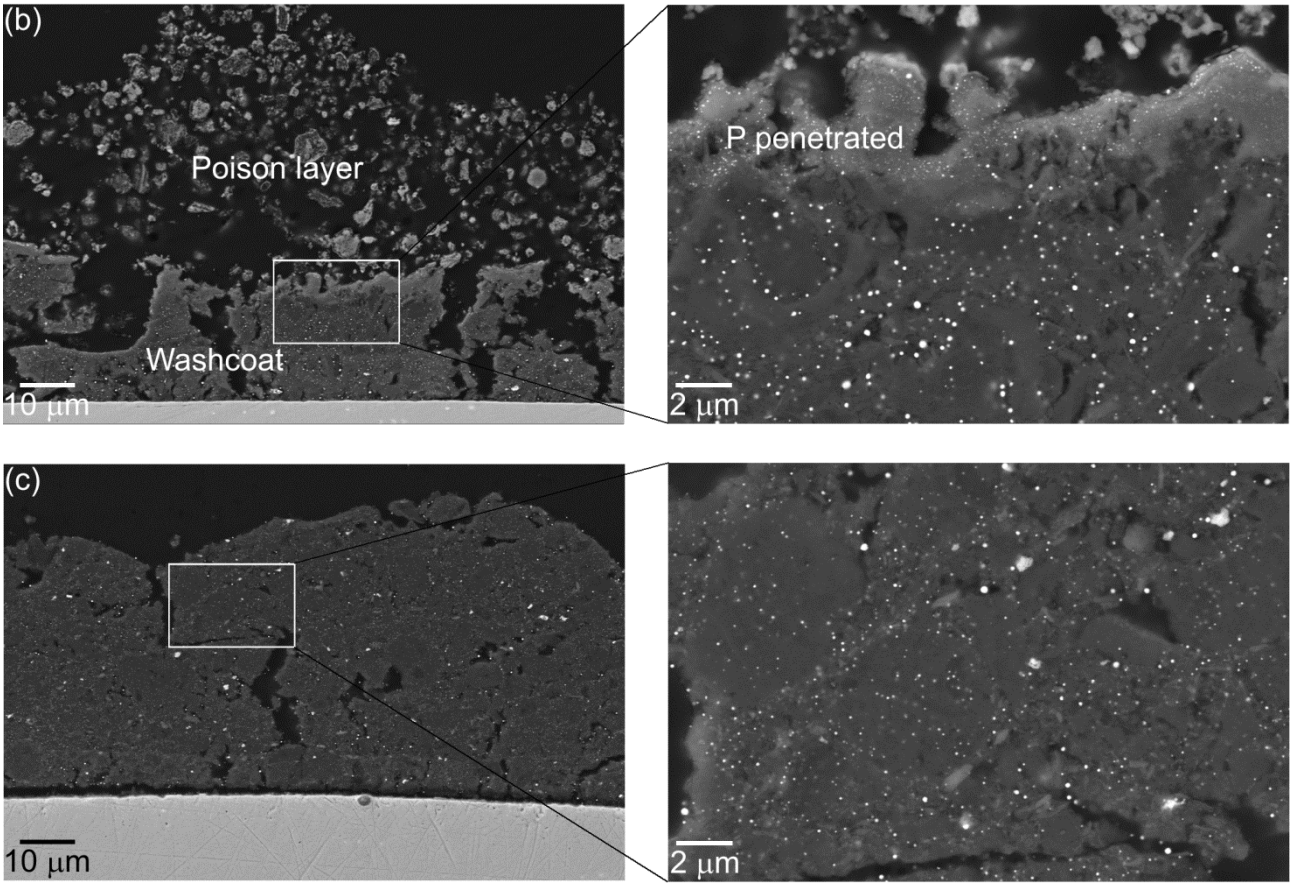

Fig. 2 Cross-sectional FEGSEM AsB images with two magnifications of the (a) fresh catalyst, (b) inlet part of the vehicle-aged catalyst (position 0, Fig. 1), and (c) middle part of the vehicle-aged catalyst (position 4, Fig. 1); white spots represent the noble metal particles

The particle size of noble metals in the vehicle-aged catalyst was measured from TEM images. Totally from 150 up to 300 particles per sample were measured. The particle sizes were measured from positions 1, 2, 4, 6, and 8 (marked in Fig. 1). It is important to notice that particles with size of 5–20 nm also existed in the catalyst samples but only particles with the size >20 nm were taken into account in the measurements. Thus, in the results there is a bias towards the bigger particle size. However, the results can be used in comparison of the particle size distributions in different sections of the catalyst. The particle size distribution in the different sections of the vehicle-aged catalyst is presented in Fig. 3. The calculated average sizes of the particles for sample positions of 1, 2, 4, 6, and 8 were 120±90 nm, 110±60 nm, 80±40 nm, 60±50 nm, and 40±10 nm, respectively. In general, noble metal particle size increases with increasing aging temperature, as reported by e.g. [21–22].

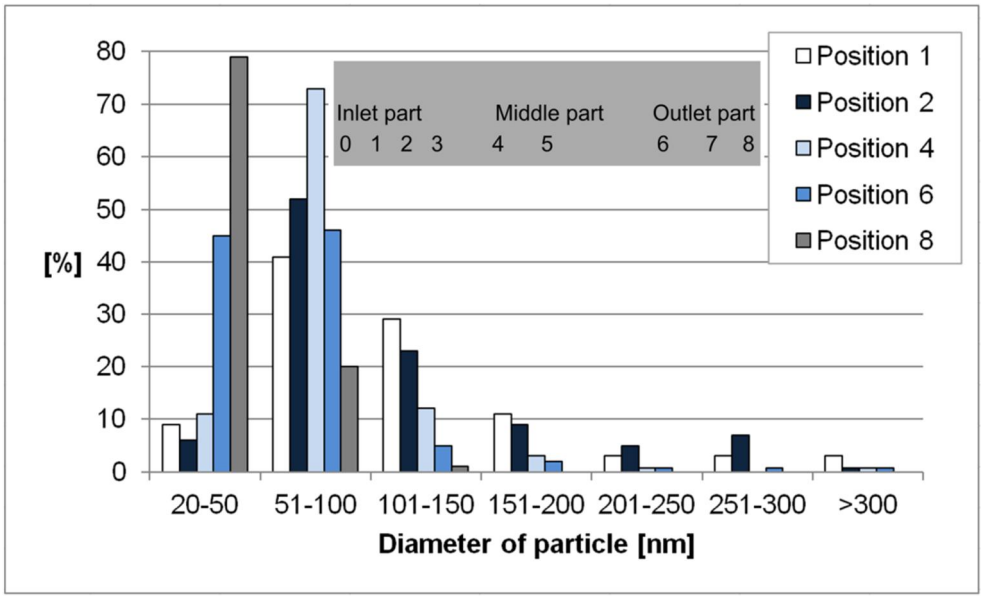

Fig. 3 Particle size distribution in different sections (positions 1, 2, 4, 6, and 8, Fig. 1) of the vehicle-aged catalyst; notice that particles with the sizes of 5–20 nm also existed, but only particles with the size >20 nm were taken into account in the measurements

More detailed structural characterization of the fresh and used catalysts was carried out with TEMs, XRD, and XPS. TEM image with SAED pattern and FEG HRTEM image of the fresh catalyst are presented in Figs. 4 (a) and (b), respectively. The fresh catalyst had a small-grained g-alumina-based washcoat with uniformly distributed, small-grained (<5 nm) Pt/Pd particles. According to EDS point analysis in the FEG HRTEM, the noble metal particles contain both Pt and Pd. Based on the XRD studies of the fresh catalyst (Fig. 5), palladium and platinum were as an oxide form. The XPS spectrum of the fresh catalyst for Pd 3d is presented in Fig. 6 (a), showing that the binding energy of Pd $3d_{5/2}$ is 337 eV which indicates palladium to be as an oxide form and can be presented possible as a mixture of PdO and PdO_2 [17]. The XPS spectrum of the fresh catalyst for Pt 4d is presented in Fig. 6 (b), showing that the binding energy of Pt $4d_{5/2}$ is 316 eV which indicates oxidized Pt in the fresh catalyst [23–25].

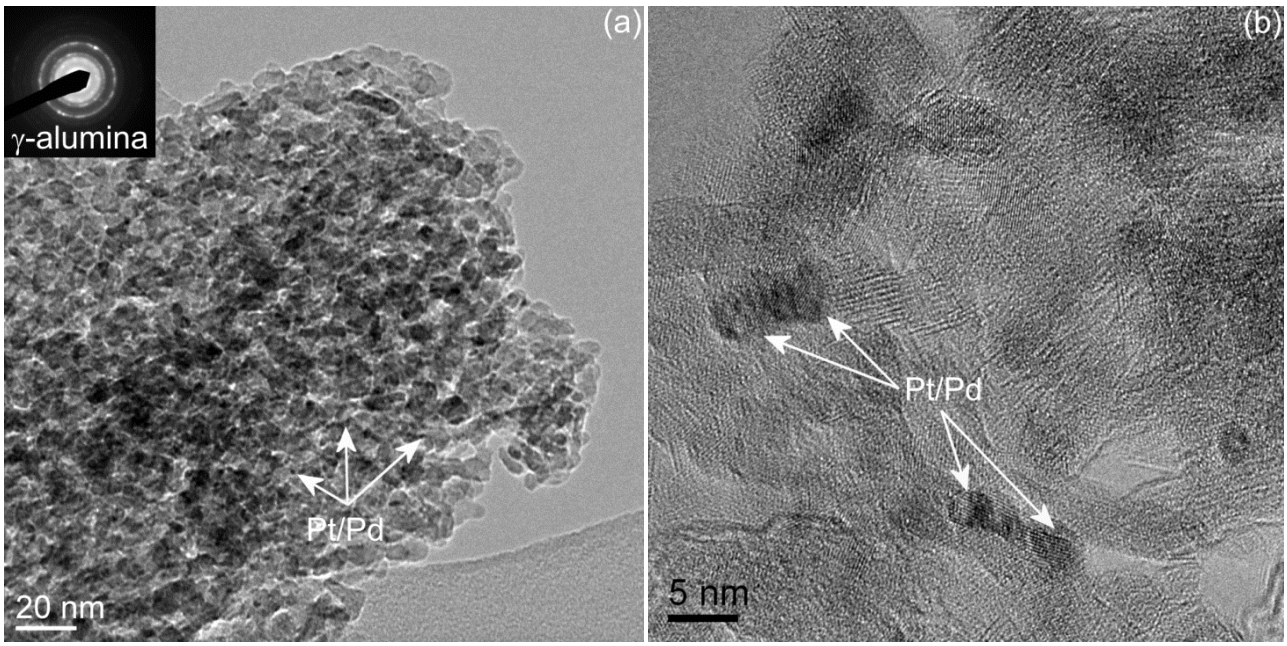

Fig. 4 The fresh catalyst, (a) TEM image with SAED pattern and (b) FEG HRTEM image

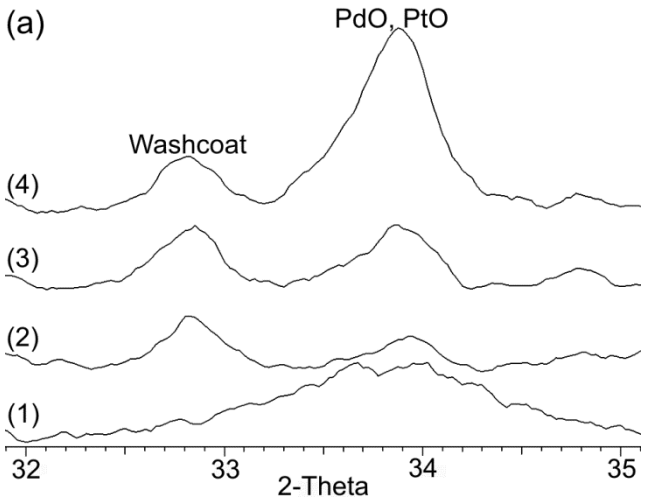

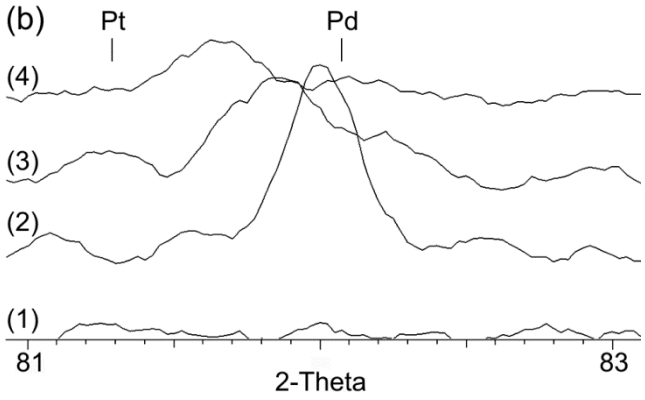

Fig. 5 XRD spectra of the catalyst samples, (a) 2θ is 32–35° and (b) 2θ is 81–83°; (1) is the fresh catalyst, (2) is the inlet part of the vehicle-aged catalyst, (3) is the middle part of the vehicle-aged catalyst, and (4) is the outlet part of the vehicle-aged catalyst

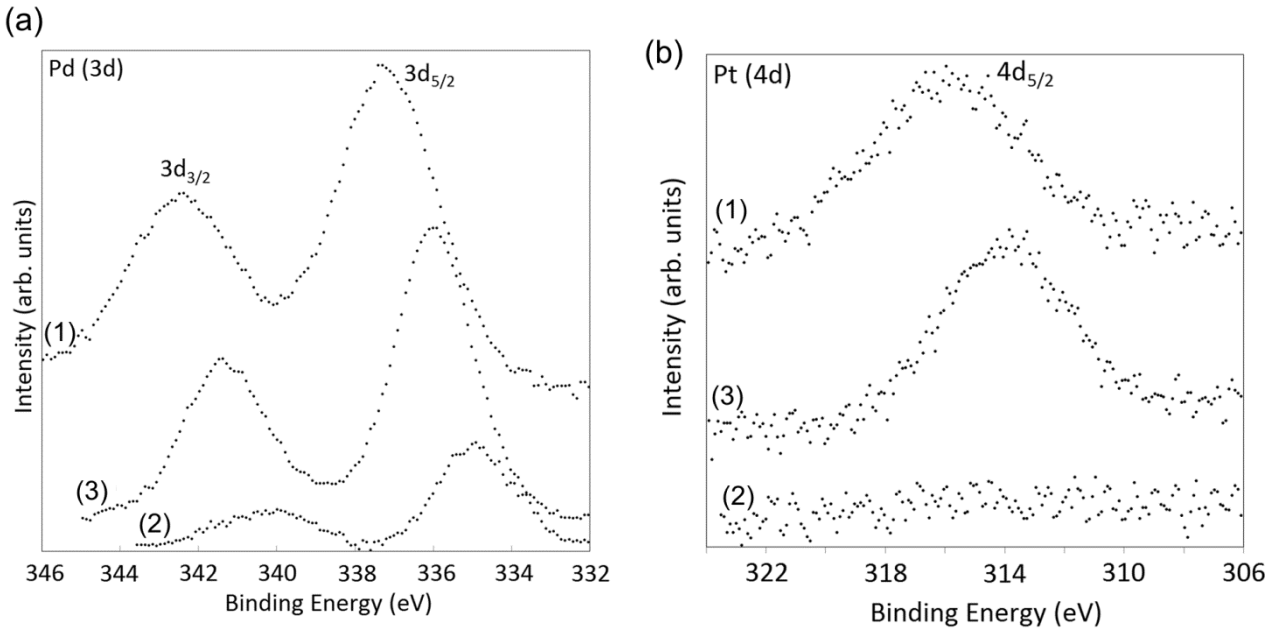

Fig. 6 XPS (a) Pd (3d) spectra and (b) Pt (4d) spectra of the catalyst samples; (1) is the fresh catalyst, (2) is the inlet part of the vehicle-aged catalyst, and (3) is the outlet part of the vehicle-aged catalyst

TEM images with various magnifications of the vehicle-aged catalyst from the inlet, middle, and outlet parts of the converter are presented in Figs. 7, 8, and 9, respectively, Figs. 7–9 include also SAED patterns of the washcoats / noble metal particle. In general, during vehicle aging Pt/Pd

particles grew significantly (Figs. 7 (a), 8 (a), and 9 (a)) compared to the fresh sample (Fig. 4 (a)) and the growing was more in the inlet than in the outlet part of the catalyst; as already seen in the particle size distribution (Fig. 3). In addition, the grain size of the washcoat increased but the structure remained the same, g-alumina, as in the fresh catalyst.

According to TEM studies of the inlet part of the used catalyst (Fig. 7), two types of the noble metal particles were detected: mainly bimetallic Pt/Pd particles with fcc structure (Fig. 7 (b)) but also bimetallic Pt/Pd particles with a Pd-rich shell (Fig. 7 (c)). According to the point EDS analysis, the composition of the bimetallic Pt/Pd particles (in Fig. 7 (b)) varied; the cores contained both Pt and Pd with Pd-rich composition but the outermost parts of the particles were even more Pd-rich. This is probably due to segregation of Pd onto the surface of the bimetallic Pt/Pd particle [26]. According to XRD studies, a peak between metallic Pd and Pt (Fig. 5 (b)) was detected indicating Pt/Pd alloy [17]. The peak was near metallic Pd indicating that the composition of bimetallic Pt/Pd was Pd-rich which agrees with the EDS analyses. These results indicate decomposition of palladium and platinum oxides followed by formation of Pd-rich bimetallic Pt/Pd particles. Datye *et al.* [5] found that decomposition of PdO starts by forming small domains of Pd on the PdO surface, Persson *et al.* [17] reported that in the thermal decomposition of PdO, Pd is incorporated into the Pt/Pd alloy, and Saenger *et al.* [27] observed that PdO/Pt/SiO_2 converted to Pd-Pt alloy/SiO_2 at 750°C in O_2. Hauff *et al.* [28] reported that the thermal decomposition of PtO to Pt happens above 350°C and that platinum oxide is reduced, PtO to Pt and PtO_2 to PtO, also by NO at low temperatures. Oxidation of Pt by O_2 and reduction of platinum oxide by NO are competing reactions; the oxidation is slower at low temperatures but at higher temperatures it is faster than the reduction [28]. Another type of the noble metal particles in the inlet part of the used catalyst was bimetallic Pt/Pd particle with a Pd-rich shell (Fig. 7 (c)). According to the SAED patterns and based on the papers by e.g. [29–32], the structure of Pd-rich shell looks to be polycrystalline palladium oxide. A small peak of PdO (Fig. 5 (a)) was detected also in the XRD spectrum of the inlet part of the used catalyst. It can be concluded

that reformation of palladium oxide has started on the Pt/Pd particle surfaces where Pd has segregated. According to XPS studies, the binding energy of Pd $3d_{5/2}$ was 335 eV (Fig. 6 (b)) corresponding to metallic Pd [8,33]. Based on TEM and XRD studies, the portion of palladium oxide was significantly less than that of bimetallic Pt/Pd. Platinum was invisible in the XPS spectrum (Fig. X (b)) due to the segregation of Pd onto the surface of the bimetallic Pt/Pd particles and due to the existence of palladium oxide on the surfaces of the Pt/Pd particles. So, it can be concluded that after decomposition of palladium oxide and platinum oxide, bimetallic Pt/Pd particles with Pd-rich composition formed. The particles had even more Pd-rich surface due to segregation of Pd onto the surface of the Pt/Pd particles. Further, reformation of palladium oxide occurred on the portion of the Pt/Pd particles. It is very likely that the operating temperature in the inlet part of the catalyst has been such that the decomposition of palladium and platinum oxides occurred and afterwards temperature has decreased so that the reformation of palladium oxide existed. In addition of high temperature, e.g. strong poisoning and mechanical stresses caused significant aging in the inlet part of the catalyst.

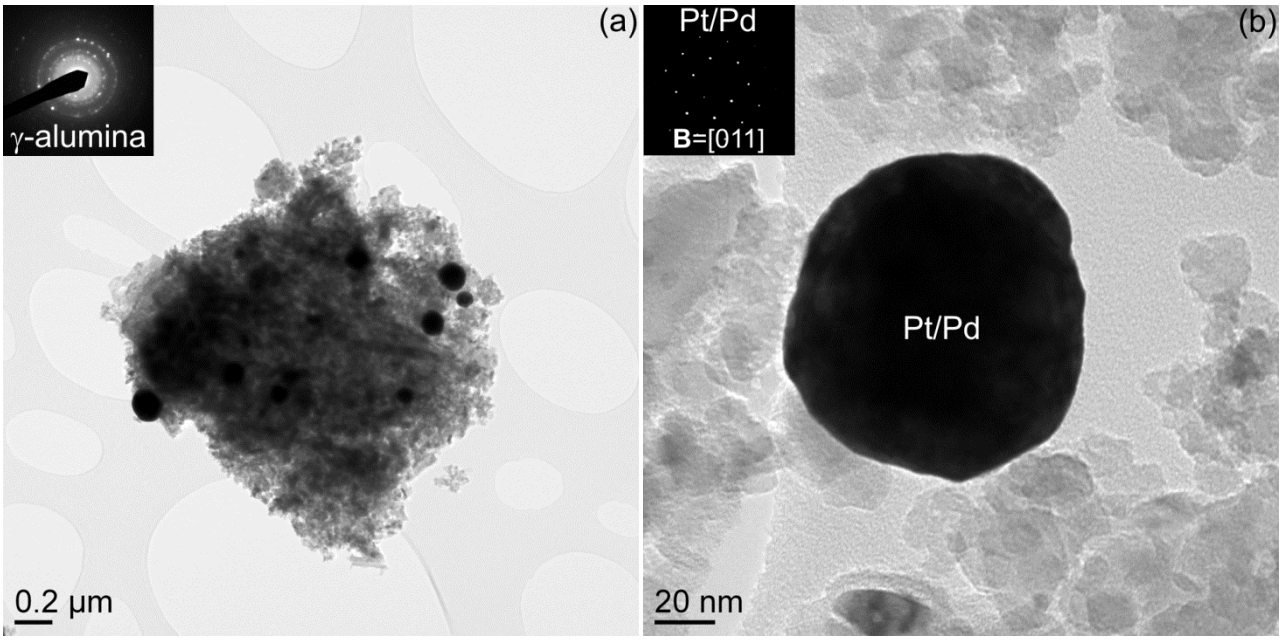

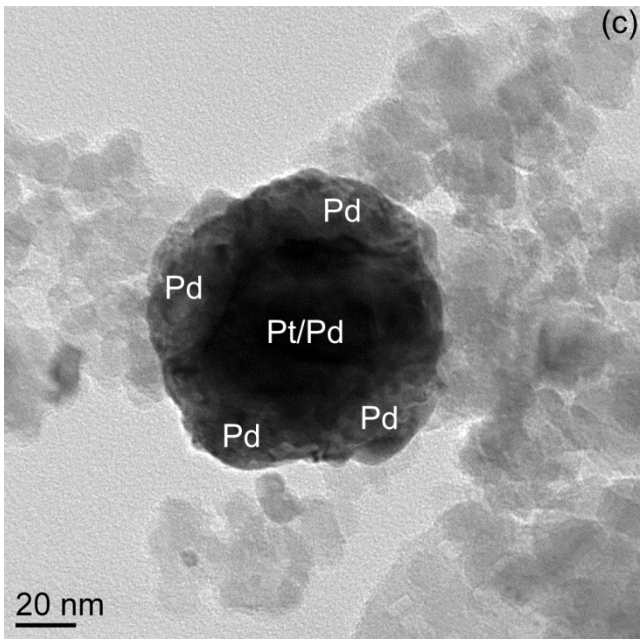

Fig. 7 The inlet part of the vehicle-aged catalyst (position 1, Fig. 1), (a) TEM image and SAED pattern of washcoat, (b) TEM image and SAED pattern of bimetallic Pt/Pd particle and (c) TEM image of bimetallic Pt/Pd particle with Pd-rich shell

According to the TEM studies of the middle part of the used catalyst (Fig. 8), the noble metal particle consisted of several crystals (Fig. 8 (b)). Bright-field STEM images with the EDS line analysis of the two noble metal particles in the middle part of the used catalyst are presented in Fig. 8 (c). Based on the EDS point and line analyses and SAED, the darker area in the TEM image (Fig. 8 (b)) and the brighter area in the bright-field STEM images (Fig. 8 (c)) of the particle are bimetallic Pt/Pd and the brighter areas in the TEM image (Fig. 8 (b)) and the darker areas in the bright-field STEM images (Fig. 8 (c)) are Pd-rich. The FEG HRTEM image of the interface of the Pt/Pd crystal and Pd-rich crystal is presented in Fig. 8 (d) showing that they are in very close contact with each other and that both crystals are single crystals. The peaks corresponding to PdO and Pt/Pd-alloy were detected in the XRD spectra (Fig. 5) and the composition of Pt/Pd-alloy was Pd-rich which agrees with the EDS point analyses. Pd-rich areas in the TEM images (Fig. 8 (b)–(d)) can be determined with XRD to be palladium oxide. Operating conditions in the middle part of the used catalyst have been such that platinum oxide has decomposed and the decomposition process of

palladium oxide has started but has been incomplete and due to that, the noble metal particles consisted of Pd-rich bimetallic Pd/Pt crystal and palladium oxide crystals.

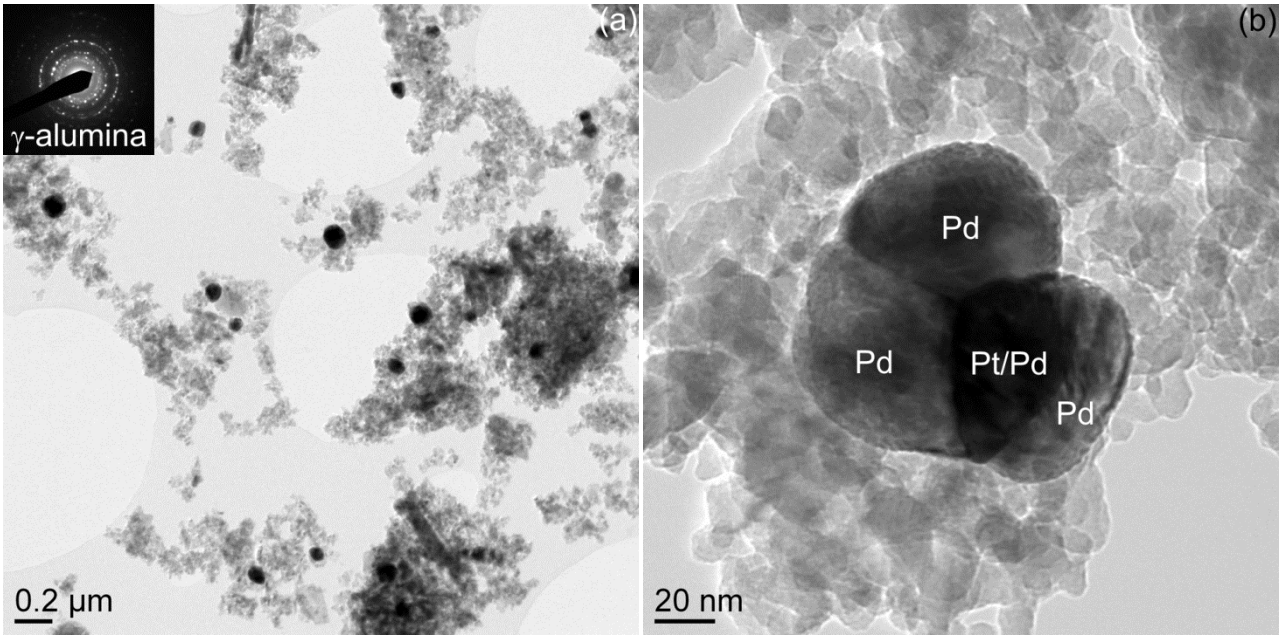

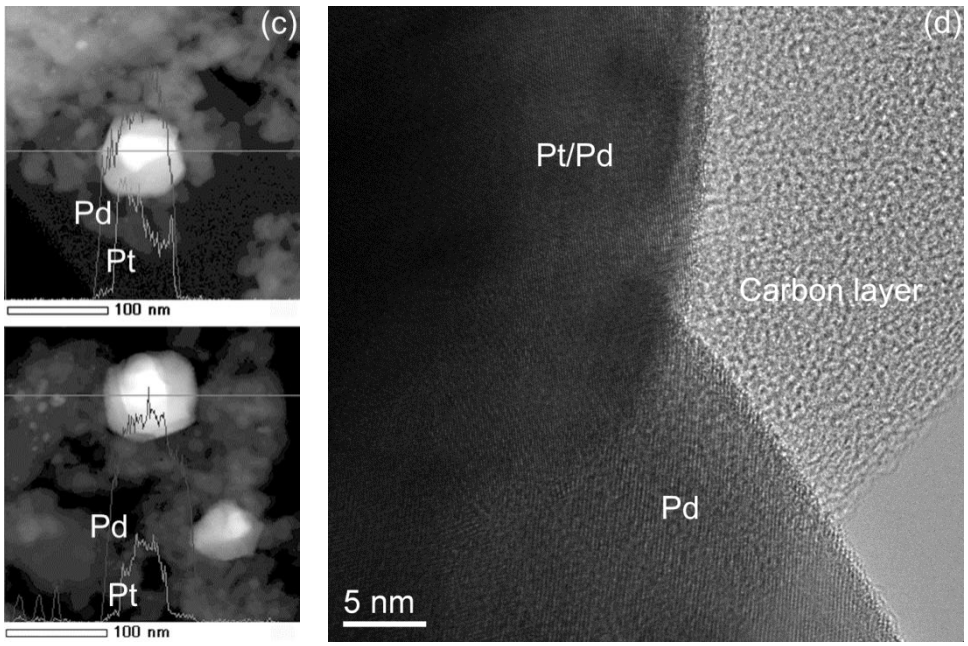

Fig. 8 The middle part of the vehicle-aged catalyst (position 4, Fig. 1), (a) TEM image and SAED pattern of the washcoat, (b) TEM image of the noble metal particle with bimetallic Pt/Pd crystal and Pd-rich crystals, (c) bright-field STEM images with EDS line analysis of two noble metal particles, and (d) FEG HRTEM image of the interface of the Pt/Pd crystal and Pd-rich crystal

According to the TEM studies of the outlet part of the used catalyst (Fig. 9), two types of noble metal particles were detected: similar to the noble metal particles in the middle part of the catalyst (Fig. 9) consisting of Pt/Pd and palladium oxide but with smaller particle sizes (Fig. 9 (b)) and Pd-rich particles (Fig. 9 (c)). A strong PdO peak (Fig. 5 (a)) and a small peak of Pt/Pd-alloy (Fig. 5 (b)) were detected in the XRD spectra. The Pt/Pd-alloy peak was midway between metallic Pt and Pd peaks indicating equal composition of bimetallic Pt/Pd which agrees with the EDS point analyses. These results show that platinum oxide has decomposed and the decomposition of palladium oxide has been slight and only a small amount of metallic Pd has formed bimetallic Pt/Pd crystals. According to the XPS studies, the binding energy of Pd $3d_{5/2}$ was 336.0 eV (Fig. 6 (c)) corresponding to PdO [8,30] and the binding energy of Pt $4d_{5/2}$ (Fig. 7 (c)) was 314 eV

corresponding to metallic Pt [23]. Thus, Pd-rich areas (Fig. 9 (b)) and Pd-rich particles (Fig. 9 (c)) in the TEM images can be determined with XRD and XPS to be PdO. So it can be concluded that decomposition of palladium oxide has been only slight and also sintering of the noble metal particles has been less than in the inlet and middle part of the catalyst.

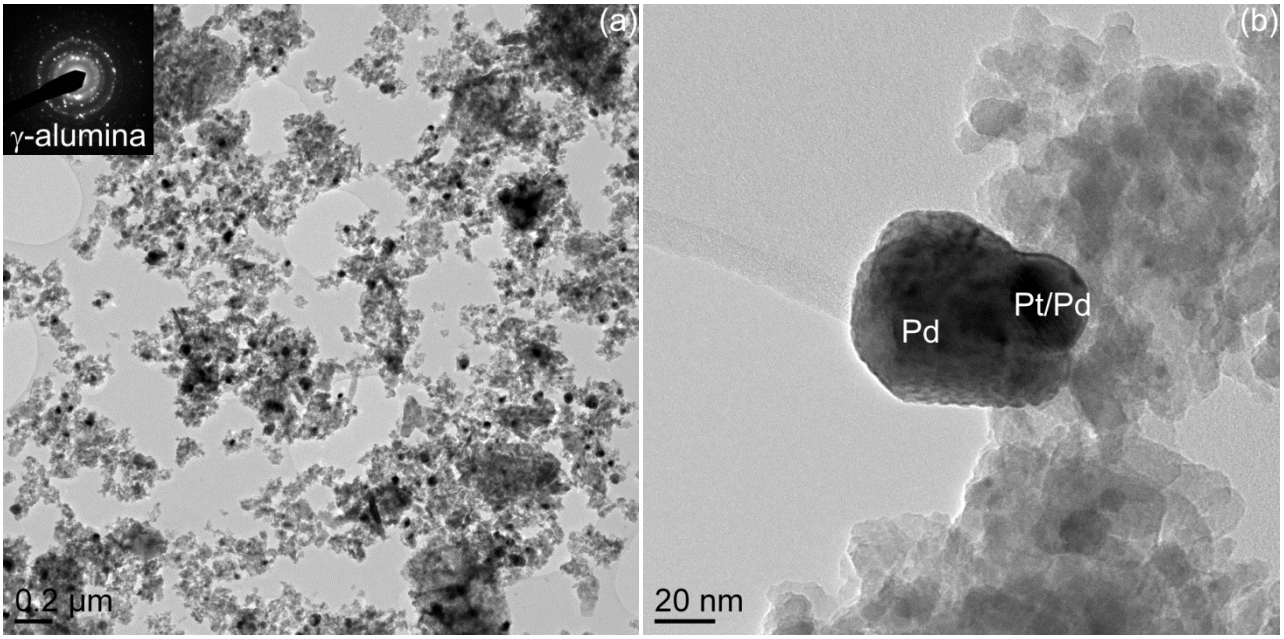

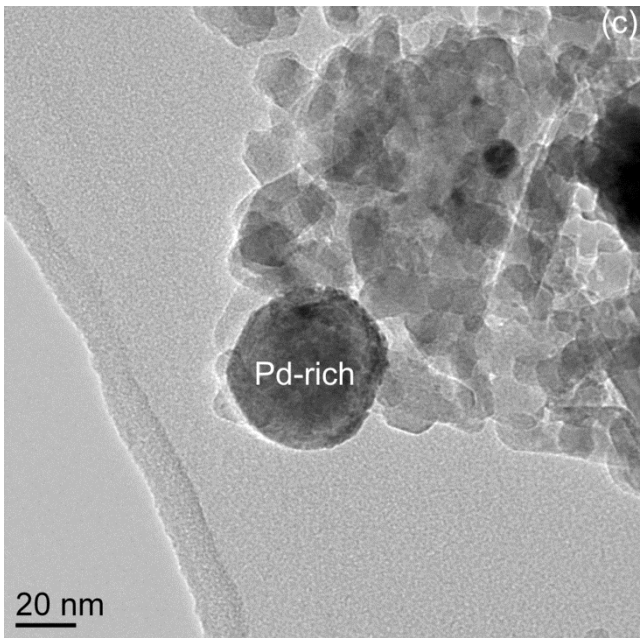

Fig. 9 The outlet part of the vehicle-aged catalyst (position 8, Fig. 1), (a) TEM image and SAED pattern of the washcoat, (b) TEM image of the noble metal particle with bimetallic Pt/Pd crystal and Pd-rich crystals, and (c) TEM image of the Pd-rich noble metal particle

3.2. Catalytic activity and catalyst surface area measurements

Catalytic activities and catalyst specific surface areas were measured for the fresh and used catalyst. Catalytic activity, CH_4 conversion as a function of temperature, of the fresh catalyst and the inlet (positions 0–3 in Fig. 1) and outlet parts (positions 6–8 in Fig. 1) of the used catalyst are presented in Fig. 10. The light-off temperature (T_{50}) of the fresh catalyst was 373°C, and that of the inlet part of the used catalyst 544°C, and the outlet part of the used catalyst 467°C. For 90% methane conversion the temperature (T_{90}) of the fresh catalyst was 459°C and that for the outlet part of the used catalyst 549°C. The inlet part of the used catalyst did not reach 90% methane conversion. So,

catalytic activity has significantly decreased in the vehicle-aged catalyst and decrease was even higher in the inlet than in the outlet part of the converter. According to the microstructural studies, it is due to many factors: a poison layer on the top of the catalyst in the inlet part, sintering of the washcoat and noble metal particles, and decomposition of active palladium oxide to Pd followed by formation of bimetallic Pt/Pd crystals. Ozawa *et al.* [12] have reported that rapid deactivation of Pt–PdO/Al_2O_3 catalyst in thermal aging at atmospheric pressure was due to the decomposition of PdO and slow deactivation due to particle growth of PdO and Pd-Pt. In the vehicle aging, in addition to thermal aging also poisons affect the deactivation of catalysts. According to the studies of the vehicle-aged catalyst, it was difficult to detect which one is more harmful, poisoning or structural changes including sintering of the washcoat and noble metal particles and decomposition of palladium oxide.

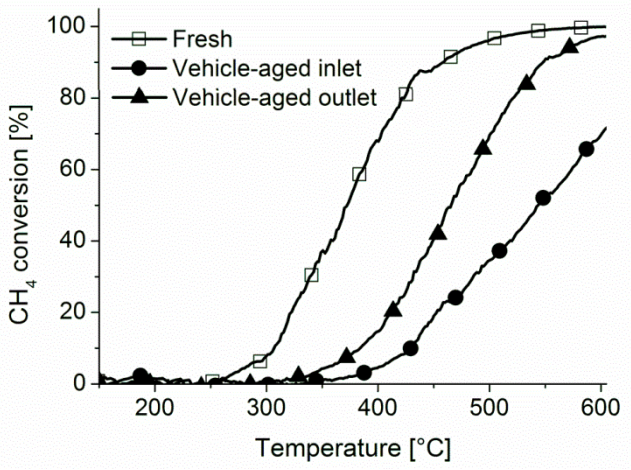

Fig. 10 Catalytic activities, CH_4 conversions, of the fresh catalyst and inlet and outlet part of the vehicle-aged catalyst; the test gas mixture contained 600 ppm CH_4, 500 ppm CO, 10 vol-% CO_2, 12 vol-% O_2 and 10 vol-% H_2O balanced with N_2

Specific surface area (S_{BET}), total pore volume, and average pore size of the fresh and used catalysts (inlet, middle, and outlet parts; positions 0–3, 4–5, and 6–8, respectively in Fig. 1) are presented in Table 1. Specific surface area and total pore volume decreased and average pore size increased during the vehicle aging. However, there is no significant difference in the results when comparing the S_{BET} and pore sizes and volumes of the samples from various positions of the used catalyst.

According to microscopical studies, poisoning of the catalyst and sintering of the washcoat and noble metal particles during the vehicle aging caused decreasing of the specific surface area.

Table 1 Specific surface area, average pore size, and total pore volume of the fresh catalyst and inlet, middle, and outlet part (positions 0–3, 4–5, and 6–8, respectively in Fig. 1) of the vehicle-aged catalyst

	Specific surface area [m^2/g]	Average pore size [nm]	Total pore volume [cm^3/g]
Fresh	154	10.1	0.37
Used inlet	53	17.5	0.22
Used middle	56	18.5	0.26
Used outlet	55	18.7	0.25

4. CONCLUSIONS

The aim of this work was to study deactivation mechanisms of the natural-gas-vehicle-aged Pt/Pd catalyst supported on the g-alumina-based washcoat. The changes compared to the fresh catalyst were studied with FEGSEM, TEM, FEG HR(S)TEM, XRD, XPS, BET-BJH, and catalytic activity measurements. In general, the grain size of the washcoat increased during the aging but its structure remained the same as in the fresh one. According to TEM, XRD, and XPS studies, in addition to the growth of the noble metal particle size, decomposition of platinum oxide and active palladium oxide to metallic Pt and Pd, respectively, followed by the formation of bimetallic Pt/Pd particles occurred. Sintering of the noble metal particles and the decomposition rate of palladium oxide were significantly less in the outlet part than in the inlet part of the used catalyst. According to the FEGSEM studies, the inlet part of the used catalyst was totally covered by a poisoning layer. These factors caused significant decreasing in the catalytic activity of the used catalyst compared to the fresh one and the activity decreased more in the inlet than in the outlet part of the used catalyst. It is difficult to conclude which is more harmful, chemical poisoning or structural changes including sintering of the washcoat and noble metal particles and the decomposition of palladium and

platinum oxides. So, it is important to study individually the effects of thermal aging and poisoning on the deactivation of the catalysts used in the natural gas applications. The achieved information based on this study can be used to develop laboratory-scale aging and poisoning methods for Pt/Pd catalysts. This information is also crucial in the development of efficient exhaust emission reduction systems for NGVs.

ACKNOWLEDGEMENTS

The authors gratefully thank the Academy of Finland for funding (Decision number 138798).

References:

[1] Gélin P, Primet M (2002) Complete oxidation of methane at low temperature over noble metal based catalysts: a review. Appl Catal B: Environ 39:1-37

[2] Holmgreen E, Yung M, Ozkan U (2007) Dual-catalyst aftertreatment of lean-burn natural gas engine exhaust. Appl Catal B: Environ 74:73-82

[3] Burch R, Urbano F (1995) Investigation of the active state of supported palladium catalysts in the combustion of methane. Appl Catal A: General 124:121-138

[4] Farrauto R, Lampert J, Hobson M, Waterman E (1995) Thermal decomposition and reformation of PdO catalysts; support effects. Appl Catal B: Environ 6:263-270

[5] Datye A, Bravo J, Nelson T, Atanasova P, Lyubovsky M, Pfefferle L (2000) Catalyst microstructure and methane oxidation reactivity during the Pd« PdO transformation on alumina supports. Appl Catal A: General 198:179-196

[6] Lyubovsky M, Pfefferle L (1999) Complete methane oxidation over Pd catalyst supported on a-alumina. Influence of temperature and oxygen pressure on the catalyst activity. Catal Today 47:29-44

[7] Lee J, Trimm D (1995) Catalytic combustion of methane. Fuel Process Tech 42:339-359

[8] Mowery D, Graboski M, Ohno T, McCormick R (1999) Deactivation of PdO-Al_2O_3 oxidation catalyst in lean-burn natural gas engine exhaust: aged catalyst characterization and studies of poisoning by H_2O and SO_2. Appl Catal B: Environ 21:157-169

[9] Yu T-C, Shaw H (1998) The effect of sulphur poisoning on methane oxidation over palladium supported on g-alumina catalysts. Appl Catal B: Environ 18:105-114

[10] Gélin P, Urfels L, Primet M, Tena E (2003) Complete oxidation of methane at low temperature over Pt and Pd catalysts for the abatement of lean-burn natural gas fuelled vehicles emissions: influence of water and sulphur containing compounds. Catal Today 83:45-57

[11] Euzen P, Le Gal J-H, Rebours B, Martin G (1999) Deactivation of palladium catalyst in catalytic combustion of methane. Catal Today 47:19-27

[12] Ozawa Y, Tochihara Y, Watanabe A, Nagai M, Omi S (2004) Deactivation of Pt-PdO/Al_2O_3 in catalytic combustion of methane. Appl Catal A: General 259:1-7

[13] Narui K, Yata H, Furuta K, Nishida A, Kohtoku Y, Tokuo, M (1999) Effects of addition of Pt to PdO/Al_2O_3 catalyst on catalytic activity for methane combustion and TEM observations of supported particles. Appl Catal A: General 179:165-173

[14] Persson K, Pfefferle L, Schwartz W, Ersson A, Järås S (2007) Stability of palladium-based catalysts during catalytic combustion of methane: The influence of water. Appl Catal B: Environ 74:242-250

[15] Yamamoto H, Uchida H (1998) Oxidation of methane over Pt and Pd supported on alumina in lean-burn natural-gas engine exhaust. Catal Today 45:147-151

[16] Lapisardi G, Urfels L, Gélin P, Primet M, Kaddouri A, Garbowski E, Toppi S, Tena E (2006) Superior catalytic behaviour of Pt-doped Pd catalysts in the complete oxidation of methane at low temperature. Catal Today 117:564-568

[17] Persson K, Jansson K, Järås S (2007) Characterisation and microstructure of Pd and bimetallic Pd-Pt catalysts during methane oxidation. J Catal 245:401-414

[18] Ersson A, Kusar H, Carroni R, Griffin T, Järås S (2003) Catalytic combustion of methane over bimetallic catalysts a comparison between novel annular reactor and high-pressure reactor. Catal Today 83:265-277

[19] Castellazzi P, Groppi G, Forzatti P (2010) Effect of Pt/Pd ratio on catalytic activity and redox behaviour of bimetallic Pt-Pd/Al_2O_3 catalysts for CH_4 combustion. Appl Catal B: Environ 95:303-311

[20] Ezekoye O, Drews A, Jen H, Kudla R, McCabe R, Sharma M, Howe J, Allard L, Graham G, Pan X (2011) Characterization of alumina-supported Pt and Pt-Pd NO oxidation catalysts with advanced electron microscopy. J Catal 280:125-136

[21] Graham G, Jen H, Ezekoye O, Kudla R, Chun W, Pan X, McCabe R (2007) Effect of alloy composition on dispersion stability and catalytic activity for NO oxidation over alumina-supported Pt-Pd catalyst. Catal Lett 116:1-8

[22] Wiebenga M, Kim C, Schmieg S, Oh S, Brown D, Kim D, Lee J-H, Peden C (2012) Deactivation mechanisms of Pt/Pd-based diesel oxidation catalysts. Catal Today 184:197-204

[23] Shyu J, Otto K (1988) Identification of platinum phases on g-alumina by XPS. Appl Surf Sci 32:246-252

[24] Serrano-Ruiz J, Huber G, Sánchez-Castillo M, Dumesic J, Rodríguez-Reinoso F, Sepúlveda-Escribano A (2006) Effect of Sn addition to $Pt/CeO_2–Al_2O_3$ and Pt/Al_2O_3 catalysts: An XPS, ^{119}Sn Mössbauer and microcalorimetry study. J Catal 241:378-388

[25] Olsson L, Fridell E (2002) The influence of Pt oxide formation and Pt dispersion on the reactions NO_2 « NO + ½ O_2 over Pt/Al_2O_3 and $Pt/BaO/Al_2O_3$. J Catal 210:340-353

[26] Yoshimura Y, Toba M, Matsui T, Harada M, Ichihashi Y, Bando K, Yasuda H, Ishihara H, Morita Y, Kameoka T (2007) Active phases and sulphur tolerance of bimetallic Pd-Pt catalysts used for hydrotreatment. Appl Catal A: General 322:152-171

[27] Saenger K, Cabral C, Duncombe R, Grill A, Neumayer D (2000) Oxygen stoichiometry in PdO_x and PdO_x/Pt electrode layers during processing of ferroelectric and high-epsilon perovskites. J Mater Res 15:961-966

[28] Hauff K, Tuttlies U, Eigenberger G, Nieken U (2012) Platinum oxide formation and reduction during NO oxidation on a diesel oxidation catalyst – Experimental results. Appl Catal B: Environ 123-124:107-116

[29] Chen M, Schmidt L (1979) Morphology and composition of Pt-Pd alloy crystallites on SiO_2 in reactive atmospheres. J Catal 56:198-218

[30] Persson K, Ersson A, Jansson K, Fierro J, Järås S (2006) Influence of molar ratio on Pd-Pt catalysts for methane combustion. J Catal 243:14-24

[31] Penner S, Wang D, Jenewein B, Gabasch H, Kötzer B, Knop-Gericke A, Schlögl R, Hayek K (2006) Growth and decomposition of aligned and ordered PdO nanoparticles. J Chem Phys 125: 094703

[32] Morlang A, Neuhausen U, Klementiev K, Schütze F-W, Miehe G, Fuess H, Lox E (2005) Bimetallic Pt/Pd diesel oxidation catalysts structural characterisation and catalytic behaviour. Appl Catal B: Environ 60:191-199

[33] Kim K, Gossmann A, Winograd N (1974) X-ray photoelectron spectroscopic studies of palladium oxides and the palladium-oxygen electrode. Anal Chem 46:197-200